Available online at www.sciencedirect.com
ScienceDirect
International Journal of Solids and Structures 43 (2006) 6978–6997
INTERNATIONAL JOURNAL OF SOLIDS and STRUCTURES
www.elsevier.com/locate/ijsolstr

Postbuckling of long unsymmetrically laminated composite plates under axial compression

Cezar G. Diaconu [a,1], Paul M. Weaver [b,*]

[a] *STRAERO Research Institute, Bucharest 77619, Romania*
[b] *Department of Aerospace Engineering, University of Bristol, Bristol BS8 1TR, UK*

Received 12 July 2005; received in revised form 19 January 2006
Available online 28 February 2006

Communicated by David A. Hills

Abstract

An approximate solution is given for the postbuckling of infinitely long and unsymmetrically laminated composite plates. This solution is obtained by superposing a polynomial transverse displacement given by bending due to unsymmetric laminate configurations and a simple functional representation for the buckling mode in conjunction with the Galerkin method. Nondimensional parameters are used to express the approximate solution in a very simple and clear formulation. The results given by this solution for axial compression in the longitudinal direction are compared with the results given by the nonlinear finite element method (FEM) for finite length rectangular long plates. The influence of the boundary conditions on postbuckling response is also studied. For the FEM analysis, two different simply supported boundary conditions on the long edges of the plate are considered. It is found that these two sets of boundary conditions give different results for the buckling and postbuckling finite element analysis. In most cases the FEM analysis overestimate and, respectively, underestimate the approximate closed form solution, depending on the type of simply supported boundary condition considered. Thus, the approximate solution appears useful for design purposes as an averaged quantity between the two FEM analyses. Also, it is found that the reduced bending stiffness method can be successfully used for determining the approximate solution.

Keywords: Buckling; Postbuckling; Laminated composites; Plates; Unsymmetrical configurations; Nondimensional parameters; Compression; Anisotropy

1. Introduction

Laminated composites are increasingly used for aerospace structures. It is important to establish new modeling and design methods in order to take advantage of their various layer angles and layer thicknesses for a

* Corresponding author. Tel.: +44 (0) 117 928 7698.
E-mail address: paul.weaver@bristol.ac.uk (P.M. Weaver).
[1] Reader in Structures, Head of Structure Analysis and Simulation Group.

0020-7683/$ - see front matter © 2006 Elsevier Ltd. All rights reserved.
doi:10.1016/j.ijsolstr.2006.02.017

Nomenclature

a, b length and width of plate
A_1, A_2, A terms defined by Eq. (23)
C_1, C_2, C_3, C_4 constants defined by Eq. (20)
$\mathbf{A} = (A_{ij})$ matrix of in-plane stiffnesses
$\mathbf{B} = (B_{ij})$ matrix of coupling stiffnesses
$\mathbf{D} = (D_{ij})$ matrix of out-of-plane stiffnesses
$\mathbf{A}^* = (A^*_{ij})$ matrix of in-plane flexibilities
$\mathbf{B}^* = (B^*_{ij})$ matrix of eccentricities
$\mathbf{D}^* = (D^*_{ij})$ matrix of reduced bending stiffnesses
D_{iso} quasi-isotropic Young's modulus of laminate material
E defined in Eq. (10)
E_{11}, E_{22} longitudinal and transverse Young's moduli of a unidirectional lamina
f, g transverse amplitudes
h plate thickness
K_{RS} relative stiffness defined in Eq. (27)
n number of half-waves of w in y-direction
$N_x, \overline{N}_x$ axial load and nondimensional axial load
N_{iso} buckling load for quasi-isotropic laminate
$\mathbf{N}$, $\mathbf{M}$ vectors of stress and moment resultants
$\overline{N}, \overline{M}$ nondimensional stress and moment resultants
u, v in-plane displacements in x, y-directions
u^0, v^0 in-plane displacements at reference plane in x, y-directions
u_{end}, $\bar{u}_{\text{end}}$ end shortening and nondimensional end shortening
w, $w_{\max}$ transverse displacement and maximum transverse displacement in z-direction
$\bar{u}, \bar{v}, \bar{w}, \bar{w}_1, \bar{w}_2$ nondimensional displacements
x, y, z Cartesian coordinates
$\bar{x}, \bar{y}, \bar{z}$ nondimensional Cartesian coordinates
α_A, β_A, γ_A, δ_A, η_A in-plane nondimensional parameters
α_D, β_D, γ_D, δ_D, η_D out-of-plane nondimensional parameters
α_B, β_B, γ_B, δ_B, η_B, μ_B, ρ_B, ω_B, ν_B, τ_B, θ_B, ζ_B coupling nondimensional parameters
$\boldsymbol{\varepsilon}^0$, $\boldsymbol{\kappa}$ vectors of strains and curvatures
ε strain given by the end shortening at buckling load for quasi-isotropic laminate
ε_{iso} strain given by the end shortening at buckling load for quasi-isotropic laminate
ν_{12} Poisson's ratio for a unidirectional lamina
λ half-wavelength of buckling mode
τ skew of the buckling pattern due to mechanical coupling (Fig. 1)
ψ middle surface force function
$\bar{\psi}$ nondimensional middle surface force function

wide range of structural configurations and loadings. Common structures include rectangular laminated plates, subjected to in-plane compression loading.

It is well known that laminated composite plates subjected to axial compression are able to carry considerable load beyond buckling. For laminated composite plates with unsymmetric laminate configurations buckling and postbuckling events are complex phenomena and many studies have been undertaken. Turvey and Wittrick (1973) found that, in the postbuckling regime, the symmetric and unsymmetric laminate configurations show the same slope of the load shortening curves. Latter, Harris (1975) observed that stiffness change after buckling is in most cases because of changes in the buckling mode. Chandra (1988) proposed a

simple closed form solution for analyzing the postbuckling of cross-ply laminated composite plates. However, this solution does not represent out-of-plane bending of the plate in the prebuckling range. More accurate postbuckling solutions were proposed using double sine series and/or multiple Fourier series techniques for simply supported plates with angle-ply (Chia and Prabhakara, 1974), cross-ply (Prabhakara, 1976) or general (Zhang, 1982) laminate configurations. These solutions are in most cases unable to give in-depth insight in to the postbuckling phenomenon and to explain the predictions largely because of the relatively large number of terms in the series. On the other hand, closed form solutions are in most situations approximations of the buckling and postbuckling phenomena and can offer only inexact qualitative results. However, such solutions have the advantage of simplicity and allow one to study the influence of each term in explaining the predictions and furthermore, provide rapid solutions in optimisation studies. Thus, Timoshenko (1913) proposed a simple closed form solution based on the skew of the buckling pattern for the buckling of isotropic infinitely long plates subjected to shear loadings. Kromm and Marguerre (1937) extended this solution to the postbuckling of isotropic infinitely long plates under shear and compressive loading. Later, Weaver (2004, 2006) observed that the same buckling pattern is induced by anisotropy and used the same solution for the buckling of infinitely long laminated composite plates subjected to compression or shear loadings. In a recent paper, Diaconu and Weaver (2005) extended this solution for the postbuckling of infinitely long laminated composite plates with laminate configurations that are symmetric with respect to their middle plane.

The objective of this paper is to study the postbuckling of long laminated plates with nonorthotropic laminate configurations that are also unsymmetric with respect to their middle plane. These plates are subjected to in-plane axial compression on longitudinal direction. It is important to study this type of laminated plates because they exhibit the most general type of anisotropy for laminated composites and also exhibit features that allow one to understand the postbuckling phenomena. Also, no study has been found in the literature for such plates. In order to exploit the response of the laminated plates subjected to compression, it is necessary to model and understand their behavior. In a previous study, Diaconu and Weaver (2005) developed an approximate solution for the postbuckling of symmetrically laminated plates. This solution is extended in the present paper to unsymmetrically laminated plates. The assumed transverse displacement is made of two terms corresponding to the bending due to zero moment boundary conditions and to the buckling mode, respectively. The postbuckling analysis is formulated in terms of nondimensional buckling coefficients and load factors, and an approximate closed form solution is obtained. The analysis is carried out for infinitely long plates with the two long edges simply supported. Postbuckling results for infinitely long plates are important because they provide a practical estimation and useful information in explaining the postbuckling behavior of finite length rectangular plates. In order to study and validate the approximate solution for postbuckling problem, the results obtained by the approximate solution for infinitely long plates are compared with the results obtained by finite element method (FEM) for finite length rectangular plates. The influence of the boundary conditions on postbuckling response is also studied.

2. Nondimensional parameters for postbuckling of infinite plates

The postbuckling behavior of laminated plates can be examined using the nonlinear plate equations of von Karman. Based on the von Karman assumptions, the large deflections plate equations can be derived in terms of transverse deflection w and force function ψ. This approach is preferred because leads to a system of only two differential equations. For deriving the equations in terms of transverse deflection and force function, the constitutive equation is written in a partial inverse form as:

$$\begin{Bmatrix} \boldsymbol{\varepsilon}^0 \\ \mathbf{M} \end{Bmatrix} = \begin{bmatrix} \mathbf{A}^* & \mathbf{B}^* \\ -(\mathbf{B}^*)^{\mathrm{T}} & \mathbf{D}^* \end{bmatrix} \begin{Bmatrix} \mathbf{N} \\ \boldsymbol{\kappa} \end{Bmatrix} \tag{1}$$

where $\mathbf{A}^* = \mathbf{A}^{-1}$, $\mathbf{B}^* = -\mathbf{A}^{-1}\mathbf{B}$, $\mathbf{D}^* = \mathbf{D} - \mathbf{B}\mathbf{A}^{-1}\mathbf{B}$. The force function ψ is defined by the stress resultants in vector $\mathbf{N}$:

$$N_x = -\psi_{,yy}, \quad N_y = -\psi_{,xx}, \quad N_{xy} = \psi_{,xy} \tag{2}$$

The vector of reference surface strains $\boldsymbol{\varepsilon}^{\mathbf{0}}$ at $z=0$ and the vector of curvatures $\boldsymbol{\kappa}$ are defined by

$$\varepsilon_x^0 = u_{,x}^0 + \tfrac{1}{2}w_{,x}^2, \quad \varepsilon_y^0 = v_{,y}^0 + \tfrac{1}{2}w_{,y}^2, \quad \varepsilon_{xy}^0 = u_{,y}^0 + v_{,x}^0 + w_{,x}w_{,y}, \quad \kappa_x = -w_{,xx}, \quad \kappa_y = -w_{,yy}, \quad \kappa_{xy} = -2w_{,xy} \tag{3}$$

In the view of Eqs. (1)–(3), the bending moments in vector $\mathbf{M}$ can be written in the form:

$$\begin{aligned} M_x &= -B_{11}^*\psi_{,yy} - B_{21}^*\psi_{,xx} + B_{61}^*\psi_{,xy} - D_{11}^*w_{,xx} - D_{12}^*w_{,yy} - 2D_{16}^*w_{,xy} \\ M_y &= -B_{12}^*\psi_{,yy} - B_{22}^*\psi_{,xx} + B_{62}^*\psi_{,xy} - D_{12}^*w_{,xx} - D_{22}^*w_{,yy} - 2D_{26}^*w_{,xy} \\ M_{xy} &= -B_{16}^*\psi_{,yy} - B_{26}^*\psi_{,xx} + B_{66}^*\psi_{,xy} - D_{16}^*w_{,xx} - D_{26}^*w_{,yy} - 2D_{66}^*w_{,xy} \end{aligned} \tag{4}$$

A Cartesian reference system is considered with the x and y axes oriented on the length and the width of the plate, respectively. While the plate is considered to be infinite on the x-axis, the origin of y-axis is on one side of the width of the plate as shown in Fig. 1. Thus, y takes values on the interval $[0,b]$.

The differential equation of transverse motion that governs the postbuckling of laminated plates is expressed in terms of w and ψ as:

$$\begin{aligned} &D_{11}^*w_{,xxxx} + 4D_{16}^*w_{,xxxy} + 2\left(D_{12}^* + 2D_{66}^*\right)w_{,xxyy} + 4D_{26}^*w_{,xyyy} + D_{22}^*w_{,yyyy} + B_{21}^*\psi_{,xxxx} + \left(2B_{26}^* - B_{61}^*\right)\psi_{,xxxy} \\ &\quad + \left(B_{11}^* + B_{22}^* - 2B_{66}^*\right)\psi_{,xxyy} + \left(2B_{16}^* - B_{62}^*\right)\psi_{,xyyy} + B_{12}^*\psi_{,yyyy} - \left(w_{,xx}\psi_{,yy} + w_{,yy}\psi_{,xx} - 2w_{,xy}\psi_{,xy}\right) = 0 \end{aligned} \tag{5}$$

The other expression that governs the postbuckling of laminated plates is the condition of compatibility and can be expressed in terms of w and ψ as:

$$\begin{aligned} &A_{22}^*\psi_{,xxxx} - 2A_{26}^*\psi_{,xxxy} + \left(2A_{12}^* + A_{66}^*\right)\psi_{,xxyy} - 2A_{16}^*\psi_{,xyyy} + A_{11}^*\psi_{,yyyy} - B_{21}^*w_{,xxxx} - \left(2B_{26}^* - B_{61}^*\right)w_{,xxxy} \\ &\quad - \left(B_{11}^* + B_{22}^* - 2B_{66}^*\right)w_{,xxyy} - \left(2B_{16}^* - B_{62}^*\right)w_{,xyyy} - B_{12}^*w_{,yyyy} = w_{,xy}^2 - w_{,xx}w_{,yy} \end{aligned} \tag{6}$$

Eqs. (5) and (6) constitute an eighth-order system of two equations for transverse deflection w and force function ψ. Thus, the postbuckling problem consists in determining the displacement w and the stress function ψ for Eqs. (5) and (6) in conjunction with the boundary conditions.

For a laminated composite plate, infinitely long and subjected to axial compression on x-axis, the simply supported boundary conditions on lateral edges $y=0$ and b are:

$$w = N_y = N_{xy} = M_y = 0 \tag{7}$$

It is convenient to describe the postbuckling behavior in terms of nondimensional parameters in order to cover a wide range of dimensions and material properties. Moreover, the nondimensionalization allows one to analyze and clarify the relative importance of the terms appearing in the equations or in the final solution. Using a similar procedure with that introduced by Stein (1983), the following nondimensionalization is performed on the Cartesian coordinates x and y, on the force function ψ and on the displacements u, v, and w:

$$\bar{x} = \frac{x}{\lambda}, \quad \bar{y} = \frac{y}{b}, \quad \bar{\psi} = \frac{\psi}{\sqrt{D_{11}^*D_{22}^*}}, \quad \bar{u} = \frac{\lambda}{\sqrt{A_{11}^*A_{22}^*D_{11}^*D_{22}^*}}u, \quad \bar{v} = \frac{b}{\sqrt{A_{11}^*A_{22}^*D_{11}^*D_{22}^*}}v, \quad \bar{w} = \frac{w}{\sqrt[4]{A_{11}^*A_{22}^*D_{11}^*D_{22}^*}} \tag{8}$$

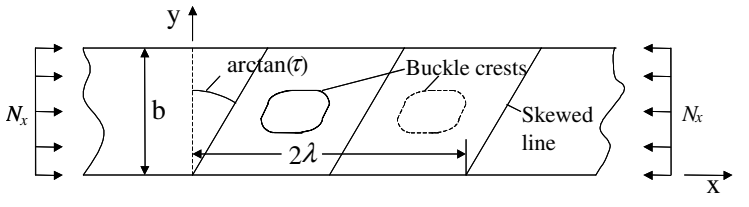

Fig. 1. Infinite plate.

and the following nondimensional parameters are introduced:

$$\alpha_A = \frac{\lambda}{b}\sqrt[4]{\frac{A_{11}^*}{A_{22}^*}},\quad \beta_A = \frac{2A_{12}^* + A_{66}^*}{2\sqrt{A_{11}^* A_{22}^*}},\quad \gamma_A = \frac{A_{16}^*}{\sqrt[4]{\left(A_{11}^*\right)^3 A_{22}^*}},\quad \delta_A = \frac{A_{26}^*}{\sqrt[4]{A_{11}^*\left(A_{22}^*\right)^3}},\quad \eta_A = \frac{A_{12}^*}{\sqrt{A_{11}^* A_{22}^*}} \tag{9a}$$

$$\alpha_D = \frac{\lambda}{b}\sqrt[4]{\frac{D_{22}^*}{D_{11}^*}},\quad \beta_D = \frac{D_{12}^* + 2D_{66}^*}{\sqrt{D_{11}^* D_{22}^*}},\quad \gamma_D = \frac{D_{16}^*}{\sqrt[4]{\left(D_{11}^*\right)^3 D_{22}^*}},\quad \delta_D = \frac{D_{26}^*}{\sqrt[4]{D_{11}^*\left(D_{22}^*\right)^3}},\quad \eta_D = \frac{D_{12}^*}{\sqrt{D_{11}^* D_{22}^*}} \tag{9b}$$

$$\alpha_B = \frac{b^2}{\lambda^2}\frac{B_{21}^*}{\sqrt[4]{A_{11}^* A_{22}^* D_{11}^* D_{22}^*}},\quad \beta_B = \frac{B_{11}^* + B_{22}^* - 2B_{66}^*}{\sqrt[4]{A_{11}^* A_{22}^* D_{11}^* D_{22}^*}},\quad \gamma_B = \frac{b}{\lambda}\frac{2B_{26}^* - B_{61}^*}{\sqrt[4]{A_{11}^* A_{22}^* D_{11}^* D_{22}^*}},\quad \delta_B = \frac{\lambda}{b}\frac{2B_{16}^* - B_{62}^*}{\sqrt[4]{A_{11}^* A_{22}^* D_{11}^* D_{22}^*}} \tag{9c}$$

$$\eta_B = \frac{\lambda^2}{b^2}\frac{B_{12}^*}{\sqrt[4]{A_{11}^* A_{22}^* D_{11}^* D_{22}^*}},\quad \mu_B = \frac{B_{11}^*}{\sqrt[4]{A_{11}^* A_{22}^* D_{11}^* D_{22}^*}},\quad \rho_B = \frac{B_{22}^*}{\sqrt[4]{A_{11}^* A_{22}^* D_{11}^* D_{22}^*}},\quad \omega_B = \frac{B_{66}^*}{\sqrt[4]{A_{11}^* A_{22}^* D_{11}^* D_{22}^*}} \tag{9d}$$

$$\nu_B = \frac{\lambda}{b}\frac{B_{16}^*}{\sqrt[4]{A_{11}^* A_{22}^* D_{11}^* D_{22}^*}},\quad \tau_B = \frac{\lambda}{b}\frac{B_{62}^*}{\sqrt[4]{A_{11}^* A_{22}^* D_{11}^* D_{22}^*}},\quad \theta_B = \frac{b}{\lambda}\frac{B_{61}^*}{\sqrt[4]{A_{11}^* A_{22}^* D_{11}^* D_{22}^*}},\quad \zeta_B = \frac{b}{\lambda}\frac{2B_{26}^*}{\sqrt[4]{A_{11}^* A_{22}^* D_{11}^* D_{22}^*}} \tag{9e}$$

where subscripts A, B and D denote, respectively, in-plane, coupling, and out-of-plane nondimensional parameters. By introducing the terms from Eqs. (8) and (9) into Eq. (5), the equation of transverse motion can now be written in terms of nondimensional parameters as:

$$\begin{aligned} E = {} & \frac{1}{\alpha_D^2}\bar{w}_{,\bar{x}\bar{x}\bar{x}\bar{x}} + 4\frac{\gamma_D}{\alpha_D}\bar{w}_{,\bar{x}\bar{x}\bar{x}\bar{y}} + 2\beta_D\bar{w}_{,\bar{x}\bar{x}\bar{y}\bar{y}} + 4\alpha_D\delta_D\bar{w}_{,\bar{x}\bar{y}\bar{y}\bar{y}} + \alpha_D^2\bar{w}_{,\bar{y}\bar{y}\bar{y}\bar{y}} + \alpha_B\bar{\psi}_{,\bar{x}\bar{x}\bar{x}\bar{x}} + \gamma_B\bar{\psi}_{,\bar{x}\bar{x}\bar{x}\bar{y}} + \beta_B\bar{\psi}_{,\bar{x}\bar{x}\bar{y}\bar{y}} \\ & + \delta_B\bar{\psi}_{,\bar{x}\bar{y}\bar{y}\bar{y}} + \eta_B\bar{\psi}_{,\bar{y}\bar{y}\bar{y}\bar{y}} - (\bar{w}_{,\bar{x}\bar{x}}\bar{\psi}_{,\bar{y}\bar{y}} + \bar{w}_{,\bar{y}\bar{y}}\bar{\psi}_{,\bar{x}\bar{x}} - 2\bar{w}_{,\bar{x}\bar{y}}\bar{\psi}_{,\bar{x}\bar{y}}) = 0 \end{aligned} \tag{10}$$

Also, the condition of compatibility in Eq. (9) becomes:

$$\begin{aligned} & \frac{1}{\alpha_A^2}\bar{\psi}_{,\bar{x}\bar{x}\bar{x}\bar{x}} - 2\frac{\delta_A}{\alpha_A}\bar{\psi}_{,\bar{x}\bar{x}\bar{x}\bar{y}} + 2\beta_A\bar{\psi}_{,\bar{x}\bar{x}\bar{y}\bar{y}} - 2\alpha_A\gamma_A\bar{\psi}_{,\bar{x}\bar{y}\bar{y}\bar{y}} + \alpha_A^2\bar{\psi}_{,\bar{y}\bar{y}\bar{y}\bar{y}} \\ & - (\alpha_B\bar{w}_{,\bar{x}\bar{x}\bar{x}\bar{x}} + \gamma_B\bar{w}_{,\bar{x}\bar{x}\bar{x}\bar{y}} + \beta_B\bar{w}_{,\bar{x}\bar{x}\bar{y}\bar{y}} + \delta_B\bar{w}_{,\bar{x}\bar{y}\bar{y}\bar{y}} + \eta_B\bar{w}_{,\bar{y}\bar{y}\bar{y}\bar{y}}) = \bar{w}_{,\bar{x}\bar{y}}^2 - \bar{w}_{,\bar{x}\bar{x}}\bar{w}_{,\bar{y}\bar{y}} \end{aligned} \tag{11}$$

Eqs. (10) and (11) in conjunction with the boundary conditions allow one to calculate the nondimensional transverse displacement $\bar{w}$ and the nondimensional stress function $\bar{\psi}$ for the postbuckling problem.

In order to determine the nondimensional in-plane displacements $\bar{u}$ and $\bar{v}$, it is necessary to replace the reference surface strains in Eq. (3) and the stress resultants in Eq. (2) into the first three constitutive relations in Eq. (1). By introducing also the nondimensional terms from Eqs. (8) and (9) into these three constitutive equations the following system is obtained:

$$\begin{cases} \bar{u}_{,\bar{x}} = \alpha_A^2\bar{\psi}_{,\bar{y}\bar{y}} + \eta_A\bar{\psi}_{,\bar{x}\bar{x}} - \alpha_A\gamma_A\bar{\psi}_{,\bar{x}\bar{y}} - \mu_B\bar{w}_{,\bar{x}\bar{x}} - \eta_B\bar{w}_{,\bar{y}\bar{y}} - \nu_B\bar{w}_{,\bar{x}\bar{y}} - \frac{1}{2}\bar{w}_{,\bar{x}}^2 \\ \bar{v}_{,\bar{y}} = \eta_A\bar{\psi}_{,\bar{y}\bar{y}} + \frac{1}{\alpha_A^2}\bar{\psi}_{,\bar{x}\bar{x}} - \frac{\delta_A}{\alpha_A}\bar{\psi}_{,\bar{x}\bar{y}} - \alpha_B\bar{w}_{,\bar{x}\bar{x}} - \rho_B\bar{w}_{,\bar{y}\bar{y}} - \zeta_B\bar{w}_{,\bar{x}\bar{y}} - \frac{1}{2}\bar{w}_{,\bar{y}}^2 \\ \bar{u}_{,\bar{y}} + \bar{v}_{,\bar{x}} = \alpha_A\gamma_A\bar{\psi}_{,\bar{y}\bar{y}} + \frac{\delta_A}{\alpha_A}\bar{\psi}_{,\bar{x}\bar{x}} + 2(\eta_A - \beta_A)\bar{\psi}_{,\bar{x}\bar{y}} - \theta_B\bar{w}_{,\bar{x}\bar{x}} - \tau_B\bar{w}_{,\bar{y}\bar{y}} - \omega_B\bar{w}_{,\bar{x}\bar{y}} - \bar{w}_{,\bar{y}}\bar{w}_{,\bar{x}} \end{cases} \tag{12}$$

One is able to determine the nondimensional in-plane displacements $\bar{u}$ and $\bar{v}$ by integrating this system. The postbuckling problem for plates with nonsymmetric laminate configurations can now be solved in a similar manner with the problem solved by Diaconu and Weaver (2005) for plates with symmetric laminate configurations. One difference is that the coupling nondimensional parameters should be taken into consideration for solving the postbuckling problem. The second difference is that the zero moment boundary condition in Eq. (7) on the long edges of the plate at $\bar{y} = 0$ and 1 is defined as

$$\overline{M}_y = -\eta_B\bar{\psi}_{,\bar{y}\bar{y}} - \rho_B\bar{\psi}_{,\bar{x}\bar{x}} + \tau_B\bar{\psi}_{,\bar{x}\bar{y}} - \eta_D\bar{w}_{,\bar{x}\bar{x}} - \alpha_D^2\bar{w}_{,\bar{y}\bar{y}} - 2\alpha_D\delta_D\bar{w}_{,\bar{x}\bar{y}} = 0 \tag{13}$$

which may induce transverse displacement into the plate prior to buckling.

3. Approximate solution

It is well known that the unsymmetrically laminated composite plates under in-plane compression may exhibit prebuckling transverse displacement. In order to obtain an approximate solution for the postbuckling problem, we assume the nondimensional transverse displacement as being made of two terms:

$$\bar{w} = \bar{w}_1 + \bar{w}_2 \tag{14}$$

The first term $\bar{w}_1$ denotes the nondimensional transverse displacement given by the zero moment boundary conditions on the long edges of the plate and is defined as:

$$\bar{w}_1 = g\bar{y}(\bar{y} - 1) \tag{15}$$

where g denotes the amplitude due to zero moment boundary conditions. From the zero moment boundary condition in Eq. (13) we are able to determine g:

$$g = \frac{\overline{N}_x \pi^2}{2\alpha_D^2}\eta_B \tag{16}$$

where the axial load $\overline{N}_x$ define the nondimensionalized compressive load on x-axis as follows:

$$\overline{N}_x = \frac{N_x b^2}{\pi^2\sqrt{D_{11}^* D_{22}^*}} \tag{17}$$

The second term $\bar{w}_2$ denotes the nondimensional transverse displacement due to buckling and is obtained by using a simple functional representation for the buckling mode in conjunction with the Galerkin method. The nondimensionalized transverse displacement $\bar{w}_2$ is assumed to be of the form introduced by Timoshenko (1913) for isotropic plates subjected to in-plane shear:

$$\bar{w}_2 = f\sin[\pi(\bar{x} - \tau\bar{y})]\sin(\pi n\bar{y}) \tag{18}$$

where f denotes the amplitude due to buckling, n denotes the half-wave number of the buckling pattern on y-axis and τ denotes the skew of the buckling pattern due to mechanical coupling. The expression (18) satisfies the boundary condition $\bar{w} = 0$ but not the exact zero moment boundary conditions on the long edges of the plate. However, this expression enables an approximate determination of the actual relations occurring at the boundary because the average zero moment boundary conditions are satisfied (Weaver, 2006).

The problem of determining $\bar{w}_2$ is similar with the postbuckling problem solved by Diaconu and Weaver (2005) for plates with symmetric laminate configurations with the difference that the reduced bending stiffness (RBS) matrix $\mathbf{D}^*$ replaces the bending stiffness matrix $\mathbf{D}$. The second difference is that the coupling terms should be also considered. From the condition of compatibility in Eq. (11) and the in-plane boundary conditions, the nondimensional stress function is determined in the form:

$$\bar{\psi} = \frac{\overline{N}_x \pi^2}{2}\bar{y}^2 + f\{C_1\cos[\pi\bar{x} - \pi(\tau - n)\bar{y}] + C_2\cos[\pi\bar{x} - \pi(\tau + n)\bar{y}]\} + f^2\{C_3\cos[2\pi(\bar{x} - \tau\bar{y})] + C_4\cos(2\pi n\bar{y})\} \tag{19}$$

where the constants C_1, C_2, C_3 and C_4 are defined as:

$$\begin{aligned}
C_1 &= -\frac{\alpha_A^2[\alpha_B - \gamma_B(\tau - n) + \beta_B(\tau - n)^2 - \delta_B(\tau - n)^3 + \eta_B(\tau - n)^4]}{2[1 + 2\delta_A\alpha_A(\tau - n) + 2\beta_A\alpha_A^2(\tau - n)^2 + 2\gamma_A\alpha_A^3(\tau - n)^3 + \alpha_A^4(\tau - n)^4]} \\
C_2 &= \frac{\alpha_A^2[\alpha_B - \gamma_B(\tau + n) + \beta_B(\tau + n)^2 - \delta_B(\tau + n)^3 + \eta_B(\tau + n)^4]}{2[1 + 2\delta_A\alpha_A(\tau + n) + 2\beta_A\alpha_A^2(\tau + n)^2 + 2\gamma_A\alpha_A^3(\tau + n)^3 + \alpha_A^4(\tau + n)^4]} \\
C_3 &= \frac{n^2\alpha_A^2}{32(1 + 2\delta_A\alpha_A\tau + 2\beta_A\alpha_A^2\tau^2 + 2\gamma_A\alpha_A^3\tau^3 + \alpha_A^4\tau^4)} \\
C_4 &= \frac{1}{32\alpha_A^2 n^2}
\end{aligned} \tag{20}$$

Eq. (19) does not satisfy exactly the in-plane boundary conditions. However, we ignore the additional terms required for satisfying the in-plane boundary conditions because they have small values (Kromm and Marguerre, 1937).

The assumed nondimensional transverse displacement due to buckling $\bar{w}_2$ in Eq. (18) and the nondimensional stress function $\bar{\psi}$ in Eq. (19) are introduced into Eq. (10) and the Galerkin method is applied:

$$\int_0^1 \int_0^2 E \sin[\pi(\bar{x} - \tau\bar{y})] \sin(\pi n \bar{y}) \mathrm{d}\bar{x}\, \mathrm{d}\bar{y} = 0 \tag{21}$$

The result is a third order algebraic equation in f:

$$(A_1 C_1 + A_2 C_2 + A) f + 2n^2 \alpha_D^2 (C_3 + C_4) f^3 = 0 \tag{22}$$

where

$$\begin{aligned} A_1 &= -[\alpha_B - \gamma_B(\tau - n) + \beta_B(\tau - n)^2 - \delta_B(\tau - n)^3 + \eta_B(\tau - n)^4]\alpha_D^2 \\ A_2 &= [\alpha_B - \gamma_B(\tau + n) + \beta_B(\tau + n)^2 - \delta_B(\tau + n)^3 + \eta_B(\tau + n)^4]\alpha_D^2 \\ A &= 1 - 4\alpha_D\gamma_D\tau + 2\alpha_D^2\beta_D(n^2 + \tau^2) - 4\delta_D\alpha_D^3\tau(3n^2 + \tau^2) + \alpha_D^4(n^4 + 6\tau^2 n^2 + \tau^4) + \overline{N}_x\alpha_D^2 \end{aligned} \tag{23}$$

The amplitude f is obtained from Eq. (22) as:

$$f = \sqrt{\frac{A_1 C_1 + A_2 C_2 + A}{-2n^2\alpha_D^2(C_3 + C_4)}} \tag{24}$$

In order to determine the amplitude f, the parameters λ ,τ and n describing the buckling pattern should be determined first. It is assumed that the exact mode at the instant of buckling remains unchanged as the amplitude increases. This approach is much less cumbersome than an analysis based on a completely general mode of deformation (Pope, 1968) and whilst useful for initial postbuckling studies may not reflect true behavior if mode-jumping occurs. The parameters λ, τ and n are determined from Eqs. (20) and (23) by minimizing $\overline{N}_x$ for $A_1 C_1 + A_2 C_2 + A = 0$ when bifurcation occurs due to buckling. In the first approximation we can neglect the coupling parameters and the problem reduces to $A = 0$. This problem is equivalent to the problem solved by Weaver (2006) in which the RBS matrix $\mathbf{D}^*$ replaces the bending stiffness matrix $\mathbf{D}$. Also, the nondimensional in-plane displacements $\bar{u}$ and $\bar{v}$ are determined by replacing Eqs. (16), (17) and (18), (19), respectively, into Eq. (12) and integrating the system in Eq. (12):

$$\begin{aligned} \bar{u} = \frac{\pi f^2}{16} \Bigg\{ & -\left[32\left(\eta_A - 2\beta_A - \gamma_A\alpha_A\tau - \frac{2\delta_A}{\alpha_A\tau} - \frac{1}{\alpha_A^2\tau^2} \right) C_3 + \frac{1}{\tau^2} + 1 - \cos(2\pi\bar{y}) \right] \sin[2\pi(\bar{x} - \tau\bar{y})] \\ & - 2\pi x + 4\pi\tau\bar{y} - \left(\frac{\gamma_A}{\alpha_A} + 2\tau \right) \sin(2\pi\bar{y}) \Bigg\} - \left(\alpha_A^2 + \frac{\eta_B^2}{\alpha_D^2} \right) \overline{N}_x \pi^2 \bar{x} - \gamma_A \alpha_A \overline{N}_x \pi^2 \bar{y} \\ & + \frac{\pi f}{2} \Bigg\{ \Bigg\{ 2C_1 \left[\eta_A - 2\beta_A - \gamma_A\alpha_A(\tau - 1) - \frac{2\delta_A}{\alpha_A(\tau - 1)} - \frac{1}{\alpha_A^2(\tau - 1)^2} \right] \\ & + \frac{\alpha_B}{(\tau - 1)^2} - \frac{\gamma_B}{(\tau - 1)} + \rho_B - \omega_B + \tau_B(\tau - 1) \Bigg\} \sin[\pi x - \pi y(\tau - 1)] \\ & + \Bigg\{ 2C_2 \left[\eta_A - 2\beta_A - \gamma_A\alpha_A(\tau + 1) - \frac{2\delta_A}{\alpha_A(\tau + 1)} - \frac{1}{\alpha_A^2(\tau + 1)^2} \right] \\ & - \frac{\alpha_B}{(\tau + 1)^2} + \frac{\gamma_B}{(\tau + 1)} - \rho_B + \omega_B - \tau_B(\tau + 1) \Bigg\} \sin[\pi x - \pi y(\tau + 1)] \Bigg\} \end{aligned} \tag{25a}$$

$$\bar{v} = \frac{\pi f^2}{16}\left\{\tau\left[32\left(\eta_A + \frac{\delta_A}{\alpha_A\tau} + \frac{1}{\alpha_A^2\tau^2}\right)C_3 - \frac{1}{\tau^2} + 1 - \cos(2\pi y)\right]\sin[2\pi(\bar{x} - \tau\bar{y})] - 2\pi\bar{y}(1+\tau^2)\right.$$
$$\left. - \left\{1 - \cos[2\pi(\bar{x} - \tau\bar{y})] - \left(\tau^2 - \frac{\eta_A}{\alpha_A^2}\right)\right\}\sin(2\pi\bar{y})\right\} - \left(\eta_A - \frac{\rho_B\eta_B}{\alpha_D^2}\right)\overline{N}_x\pi^2\bar{y} - \frac{(2\bar{y}-1)^3}{12}g^2$$
$$+ \frac{\pi f}{2}\left\{\left\{2C_1(\tau-1)\left[\eta_A + \frac{\delta_A}{\alpha_A(\tau-1)} + \frac{1}{\alpha_A^2(\tau-1)^2}\right] + \frac{\alpha_B}{(\tau-1)} - \zeta_B + \rho_B(\tau-1)\right\}\sin[\pi x - \pi y(\tau-1)]\right.$$
$$\left. + \left\{2C_2(\tau+1)\left[\eta_A + \frac{\delta_A}{\alpha_A(\tau+1)} + \frac{1}{\alpha_A^2(\tau+1)^2}\right] - \frac{\alpha_B}{(\tau+1)} + \zeta_B - \rho_B(\tau+1)\right\}\sin[\pi x - \pi y(\tau+1)]\right\} \quad (25b)$$

For structural engineers it is important to calculate the nondimensional end shortening $\bar{u}_{\text{end}}$, which is the in-plane displacement at the end of the plate in longitudinal direction when the plate is compressed. For infinitely long plates the nondimensional end shortening $\bar{u}_{\text{end}}$ is calculated at the end of the half-wavelength as follows

$$\bar{u}_{\text{end}} = -\frac{\pi^2 f^2}{8} - \left(\alpha_A^2 + \frac{\eta_B^2}{\alpha_D^2}\right)\overline{N}_x\pi^2 \quad (26)$$

The postbuckling behavior of laminated composite plates is often investigated by calculating the slope at instant buckling of a curve relating the applied load and the end shortening, that is the deformation parallel to the undeformed middle surface on $\bar{x}$-axis. This slope, called relative stiffness, represents the stiffness immediately after buckling divided by the stiffness immediately before buckling (Harris, 1975) and allows one to calculate the end shortening of the plate for given loads without a prior determination of the amplitude f. For an infinitely long plate with unsymmetric laminate configurations and subjected to axial loads on $\bar{x}$-axis, the relative stiffness is obtained in the form:

$$K_{\text{RS}} = \frac{16(C_3+C_4)(\alpha_A^2\alpha_D^2 + \eta_B^2)}{\alpha_D^2 + 16(C_3+C_4)(\alpha_A^2\alpha_D^2 + \eta_B^2)} \quad (27)$$

Note in Eqs. (26) and (27) the nondimensional parameter η_B that shows the influence on the approximate solution of the stiffness coupling term B_{12}^* given by the nonsymmetric laminate configuration.

Another important quantity for structural engineers is the maximum nondimensional transverse displacement of the plate that can be defined easily as:

$$\bar{w}_{\max} = \frac{|g|}{4} + |f| \quad (28)$$

where $|g|/4$ is given by maximum $\bar{w}_1$ defined in Eq. (15) at $\bar{y} = 1/2$.

The solution developed in this section is called approximate because the boundary conditions and the equation of motion are not satisfied exactly. Moreover, this solution depends on the parameters given by the solution for the buckling problem that are also obtained by an approximate procedure. We can make more simplifications by employing RBS method (Ashton, 1969) for calculating the buckling load and the amplitude f in Eq. (24).

Note that in the solution developed above the transverse displacement due to zero moment boundary condition at the edges of the plate and the transverse displacement due to buckling are disconnected. This approach is consistent with the results of Turvey and Wittrick (1973) that the coupling terms do not appear to affect the postbuckled plate stiffness and they have influence mainly on the stress field within the plate and less on the deflection due to buckling. Also, this solution is based on the condition that the unsymmetrically laminated plates buckle under in-plane compression. Some studies (Lagace et al., 1986; Qatu and Leissa, 1993) made on short length rectangular plates concluded that for cross-ply configurations the bifurcation does not occur because the plates bend for any compressive load. However, no study was carried on long rectangular plates. In order to verify the validity of the approximate solution developed above and to study the postbuckling behavior of long laminated plates we will compare this approximate solution with the finite element method (FEM).

4. Comparison between the approximate solution and FEM

In this section, numerical results given by the approximate solution developed for postbuckling problem in the previous section will be compared with the numerical results given by FEM. In the approximate solution, the full analysis, that is the analysis taking into consideration all the coupling terms, and also the RBS analysis, that is, the simplified analysis employing RBS method, are both used for calculating the buckling load and the amplitude f in Eq. (24). The numerical results given by FEM are obtained for a rectangular finite plate with the aspect ratio 20. This aspect ratio is chosen in order to minimize the influence of the boundary conditions at the two ends of the plate in the longitudinal direction. Also, in the FEM model we chose the width to thickness ratio to be rather large, that is $b/h = 100$, to minimise transverse shear effects. The plate is modeled with the commercial code ABAQUS using the quadratic shell element with eight nodes S8R and a mesh of 10×400 elements. Convergence studies on the mesh size were carried out in order to find out the accuracy of the model and good results were obtained for this mesh. The compressive axial loads are distributed on the nodes at the two ends of the plate on longitudinal direction. In order to obtain transverse displacement with the FEM, we impose on the FEM model a small imperfection in the form of the first buckling mode shape and of a magnitude of 1% of the plate thickness.

As a numerical example we consider a laminated graphite/epoxy plate having the following properties for a unidirectional lamina:

$$E_{11}/E_{22} = 25, \quad G_{12}/E_{22} = 0.5, \quad \nu_{12} = 0.25 \tag{29}$$

In order to understand the influence of coupling nondimensional parameters, i.e. the coupling parameters with B subscripts, it is important to establish their range for the given material properties. Only the parameters that contribute to the maximum transverse displacement $w_{\max}$ and to the end shortening u_{end} will be analyzed. When $b = \lambda = 1$, the maximal absolute values for coupling nondimensional parameters are $|\alpha_B|, |\eta_B| \leqslant 2$, $|\delta_B|, |\gamma_B| \leqslant 5.49$ and $|\beta_B| \leqslant 4.36$. These extreme theoretical values for the nondimensional parameters cannot be reached in practice when the layer angles and thicknesses are restricted to a discrete set. The lay-ups chosen for the study have large amounts of anisotropy and relatively large values of the coupling nondimensional parameters as it can be seen in Table 1 for full analysis. For example, when $b = \lambda = 1$, for a four layers laminate with angles restricted to 0, 90 and 45 deg, the maximum $|\eta_B| = 1.645$ is obtained for a [90/90/45/−45] configuration. Note, that the number of layers is restricted to a maximum of four because those laminates with more layers usually exhibit less amounts of anisotropy.

The plate is subjected to constant axial compression on x-axis. Two quantities are considered for comparison between the approximate solution and the FEM solution. The first quantity is the maximum transverse displacement $w_{\max}$. The second quantity is the strain ε given by the end shortening u_{end} on x-direction. For the finite plate modeled with FEM, the strain ε is the ratio between the end shortening u_{end} and the length of the plate a, that is $\varepsilon = u_{\text{end}}/a$. For the infinite plate modeled by the approximate solution, the strain ε is the ratio between the end shortening u_{end} and the half-wavelength λ, that is:

$$\varepsilon = \frac{u_{\text{end}}}{\lambda} \tag{30}$$

It is well known that the postbuckling problem is highly dependant of the boundary conditions of the plate. The approximate solution was developed for infinitely long plates and does not contain information regarding the loaded ends of a rectangular long plate. On the other hand, the FEM solution is obtained for rectangular long plates with finite length. In order to compare the results given by the two solutions, it is important to understand the influence of the boundary conditions at the two loaded ends of the plate in the longitudinal direction for the FEM solution. In the first instance the FEM model is considered with all four boundaries of the plate to be simply supported, with the lateral edges of the plate allowed to have periodic in-plane displacements, that is, no straightness constraints are imposed on the edges. The loaded edges are restricted to uniform in-plane displacements.

Fig. 2 shows the normalized maximum transverse displacement $w_{\max}/h$ function of the normalized axial loads N_x/N_{cr} given by the approximate and the FEM solutions for plates with [0/90] laminate configuration. The maximum transverse displacement $w_{\max}$ is normalized with respect to the plate thickness h and the axial

Table 1
Nondimensional parameters and half-wavelengths for laminate configurations using full analysis

Laminate configuration	Nondimensional parameters					Half-wavelength
	α_B	β_B	γ_B	δ_B	η_B	λ
[0/90/0/90]	−0.0084	0	0	0	0.0084	1
[0/0/0/90]	−0.0104	0	−1.0056	0	0.0422	1.4188
[0/90/90/90]	−0.0420	0	1.0056	0	0.0104	0.7063
[0/90/90/0]	0	0	0	0	0	1.5313
[0/90]	−0.0256	0	0	0	0.0256	1
[45/−45]	0	0	−0.0247	−0.0247	0	1
[0/45]	−0.3390	1.6686	0.4219	0.6791	−0.0169	1.2687
[90/45]	−0.0206	1.6686	0.7512	0.3814	−0.2770	0.7125
[67.5/−67.5]	0	0	0.6100	−1.0607	0	0.5750
[22.5/−22.5]	0	0	−1.0655	0.6072	0	1.7313
[67.5/22.5]	0.3904	0	1.0685	−0.9266	−0.2936	0.9313
[67.5/−22.5]	0.0094	0	−0.0194	−0.0209	−0.0108	1.0375
[0/0/45/−45]	−1.0119	2.1740	0.2486	−0.5935	−0.0768	1.2750
[90/90/45/−45]	−0.0673	2.1740	−0.5558	0.2654	−1.1538	0.8375
[0/90/45/−45]	−0.3835	2.6321	−0.1806	−0.2573	−0.4716	1.1938
[90/0/45/−45]	−0.5883	2.6321	−0.2874	−0.1617	−0.3074	0.7500
[0/45/−45/90]	−0.3603	0	−0.2417	−0.2447	0.3694	1.0063
[45/0/90/−45]	−0.1606	0	−0.9819	−1.0191	0.1730	1.0188
[45/0/−45/90]	0.0096	−1.6998	−0.7815	−0.3967	0.2851	0.7125
[45/90/−45/0]	0.4488	−1.6998	−0.4977	−0.6229	0.0061	1.1187

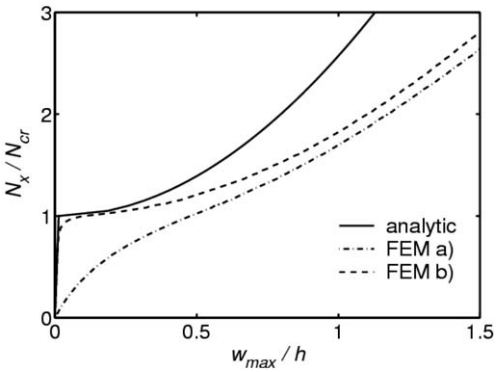

Fig. 2. Maximum transverse displacement $w_{\max}/h$ for an axially compressed [0/90] laminated plate.

loads N_x are normalized with respect to the critical buckling load $N_{\rm cr}$. The continuous line shows the results obtained with the approximate solution for an infinitely long plate regardless of the analysis considered, that is, the results are identical for the full analysis and for the RBS analysis. The dashed and dot-dashed lines show the results obtained using FEM for the finite plate. The two lines obtained with FEM correspond to respectively, (a) displacements near the longitudinal ends of the plate, and (b) displacements over the interior of the plate. In Fig. 2, one can see that the approximate solution for infinite plates underpredicts the displacements when compared with the FEM. Note that while the displacements near the ends of the plate are large for small axial loads, in the rest of the plate bifurcation occurs and the prebuckling displacements are small. This buckling pattern for the laminated plate can be also observed in Fig. 3 for three different axial loads. Fig. 3 shows the transverse displacements at $\bar{y} = 1/2$ for a plate with [0/90] laminate configuration axially compressed to $N_x = 0.5 \times N_{\rm cr}$, $N_x = 1.0 \times N_{\rm cr}$ and $N_x = 1.1 \times N_{\rm cr}$. As also observed in Fig. 2, for a load smaller than the critical buckling load $N_{\rm cr}$, the displacement is large only near the simply supported loaded ends of the plate. In effect, the amplified displacement near the loaded ends is analogous to the bending boundary layer effect in cylindrical shells.

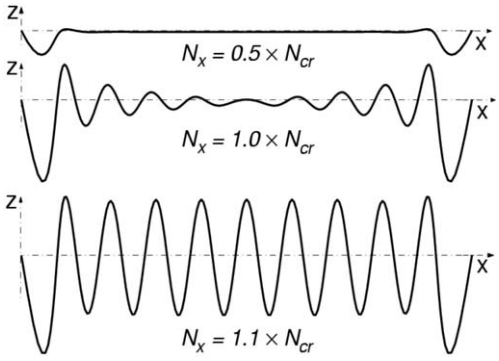

Fig. 3. Transverse displacements at $\bar{y} = 1/2$ for an axially compressed [0/90] laminated plate.

In Figs. 4–11, results given by the approximate solution and FEM analyses are compared for several laminate configurations. Clamped loaded ends replace the simply supported loaded ends in the FEM model in order to prevent the large prebuckling displacements due to the bending boundary layer effect observed in Figs. 2 and 3 near the ends of the plate because such displacements are not considered in the approximate solution. For the FEM analyses, two types of simply supported boundary conditions are considered on the lateral unloaded edges of the plate. For both FEM analyses the simply supported lateral edges are allowed to have in-plane displacements. The first FEM analysis is carried out for plates with the simply supported lateral edges without any straightness constraint imposed on them, which lead to periodic in-plane displacements of the lateral edges. In Figs. 4–11, the numerical results obtained with this analysis are noted with FEM 1 and are depicted with dashed lines. The second FEM analysis is carried out for plates with the simply supported

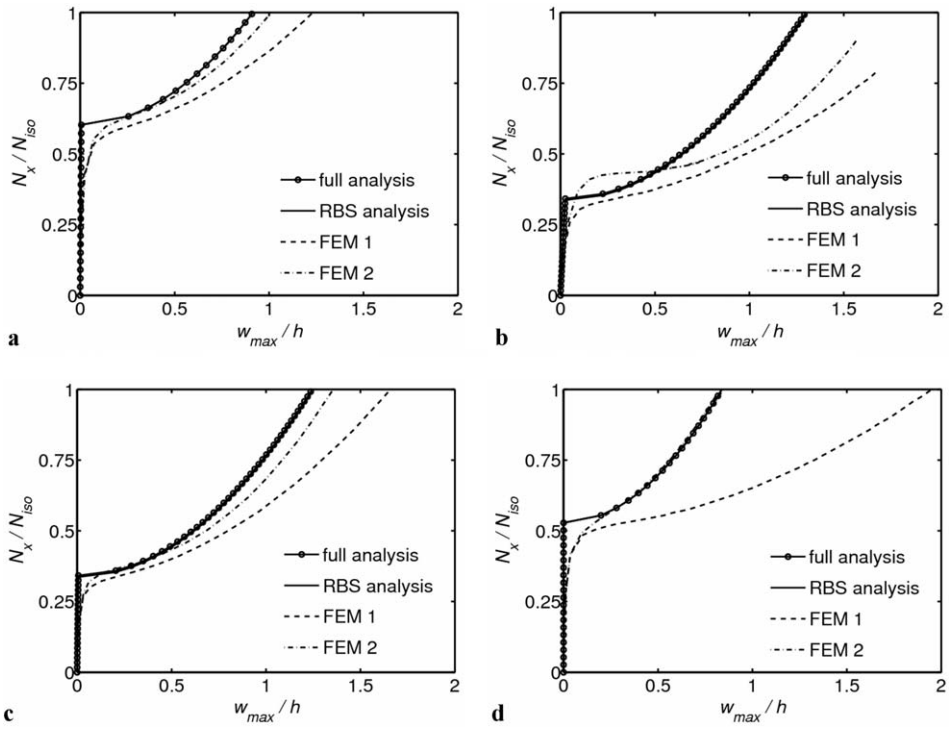

Fig. 4. Normalized maximum transverse displacement $w_{\max}/h$ function of the normalized axial loads N_x/N_{iso} for cross-ply laminates made of four layers with 0, 90 deg fiber angles: (a) [0/90/0/90], (b) [0/0/0/90], (c) [0/90/90/90] and (d) [0/90/90/0].

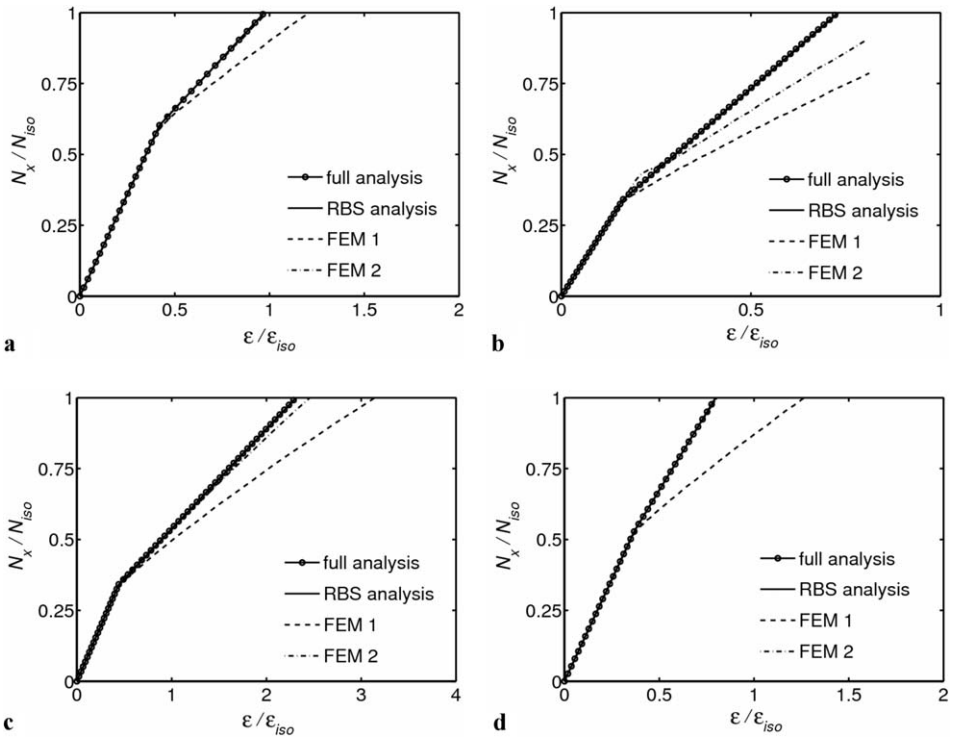

Fig. 5. Normalized strain $\varepsilon/\varepsilon_{\text{iso}}$ function of the normalized axial loads N_x/N_{iso} for cross-ply laminates made of four layers with 0, 90 deg fiber angles: (a) [0/90/0/90], (b) [0/0/0/90], (c) [0/90/90/90] and (d) [0/90/90/0].

lateral edges forced to remain straight and the numerical results obtained with this analysis are noted as FEM 2 and are depicted with dash-doted lines. It is important to consider these two analyses because no information regarding the straightness of the lateral edges is included in the approximate solution. Also in the figures, the continuous lines show the results obtained using the RBS analysis while the continuous lines with circles show the results obtained using the full analysis in the approximate closed form solution.

Fig. 4 shows the normalized maximum transverse displacement $w_{\max}/h$ function of the normalized axial load N_x/N_{iso}. The maximum transverse displacement $w_{\max}$ is normalized with respect to the plate thickness h and the axial loads N_x are normalized with respect to the critical buckling load for a quasi-isotropic laminate N_{iso}. Fig. 4 shows the results for four cross-ply laminates with four layers: [0/90/0/90], [0/0/0/90], [0/90/90/90] and [0/90/90/0]. Regarding the initial buckling loads, note that for the antisymmetric laminate configuration [0/90/0/90] in Fig. 4a the buckling load is larger than for the other four layered cross-ply configurations shown in Fig. 4 including its symmetric counterpart [0/90/90/0] in Fig. 4d. This somewhat surprising result, that an unsymmetrical laminate may have a larger buckling load than the equivalent symmetric counterpart, may be understood by examining the results presented by Weaver (2006), where the nondimensional buckling load is given by

$$\frac{N_x}{N_{\text{iso}}} = \frac{\sqrt{D_{11}^* D_{22}^*}}{D_{\text{iso}}} \frac{(1+\beta_D)}{2} \tag{31}$$

for laminates without flexural/twist anisotropy. Note that the geometric mean of principal bending stiffnesses, $(D_{11}^* D_{22}^*)^{0.5}$ for [0/90/0/90] is larger than that for [0/90/90/0] and although β_D is smaller in value for [0/90/0/90] the combined effect is one that increases the buckling load for [0/90/0/90].

For these cross-ply configurations the results given by the approximate closed form solution are identical for the full analysis and for the RBS analysis. One can see that for all cases the prebuckling displacement is very small or nonexistent and the plates always buckle. By comparing FEM 1 and FEM 2 one can see that the

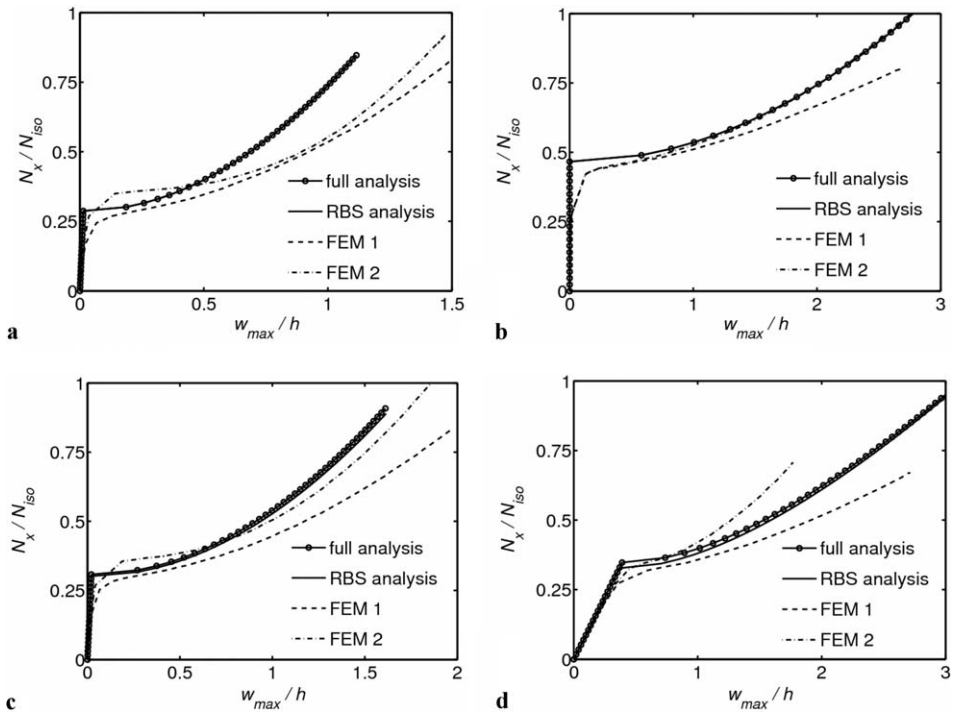

Fig. 6. Normalized maximum transverse displacement $w_{\max}/h$ function of the normalized axial loads N_x/N_{iso} for laminates made of two layers with 0, 90, 45 deg fiber angles: (a) [0/90], (b) [45/−45], (c) [0/45] and (d) [90/45].

two types of simply supported boundary conditions lead to very different postbuckling behaviors for the plates. Moreover, in Fig. 4b, for the [0/0/0/90] laminate configuration, the FEM 1 and FEM 2 results show a large difference between the buckling loads. Also, buckling load and the initial postbuckling path given by the approximate closed form solution are between the two values given by FEM analyses. Note that for [0/90/0/90] and [0/90/90/90] laminate configurations in Fig. 4a and c, respectively, the initial postbuckling path for the approximate solution match relatively well the FEM 2 results. Also, in Fig. 4d an excellent match exists between the approximate solution and the FEM 2 because the laminate configuration [0/90/90/0] is symmetric. However, Fig. 4d shows the largest difference between the FEM 1 and FEM 2 that suggests that the postbuckling behavior of the plate is highly dependent on the boundary conditions, that is, the straightness constraint imposed on the edges.

Fig. 5 shows the normalized strain $\varepsilon/\varepsilon_{\text{iso}}$ as a function of the normalized axial loads N_x/N_{iso} for the same laminate configurations as in Fig. 4. The strain ε is normalized with respect to ε_{iso}, that is the strain given by the end shortening at the buckling load for a quasi-isotropic laminate. As in Fig. 4, the results given by the approximate closed form solution are identical for the full analysis and for the RBS analysis. Excellent agreements can be observed for the prebuckling strain between the approximate solution and the FEM analyses. Also, in Fig. 5a, c and d good agreements can be observed for the initial postbuckling strain between the approximate solution and the FEM 2 analysis. For the [0/0/0/90] laminate configuration in Fig. 5b the initial postbuckling strain given by the approximate solution lies between the strains given by FEM 1 and FEM 2. Note the discrepancies for the postbuckling strain between FEM 1 and FEM 2. As in Fig. 4d, the largest discrepancy can be observed for the symmetric laminate configuration [0/90/90/0] in Fig. 5d.

Fig. 6 shows the normalized maximum transverse displacement $w_{\max}/h$ function of the normalized axial loads N_x/N_{iso} for four laminates with two layers: [0/90], [45/−45], [0/45] and [90/45]. Note that the prebuckling transverse displacement is small for [0/90] and [0/45] laminate configurations in Fig. 6a and c, respectively, and zero for the [45/−45] laminate configuration in Fig. 6b. In Fig. 6d a large prebuckling transverse displacement is observed for [90/45] laminate configuration due to a large value of η_B, that is $|\eta_B| = 0.28$ for full analysis.

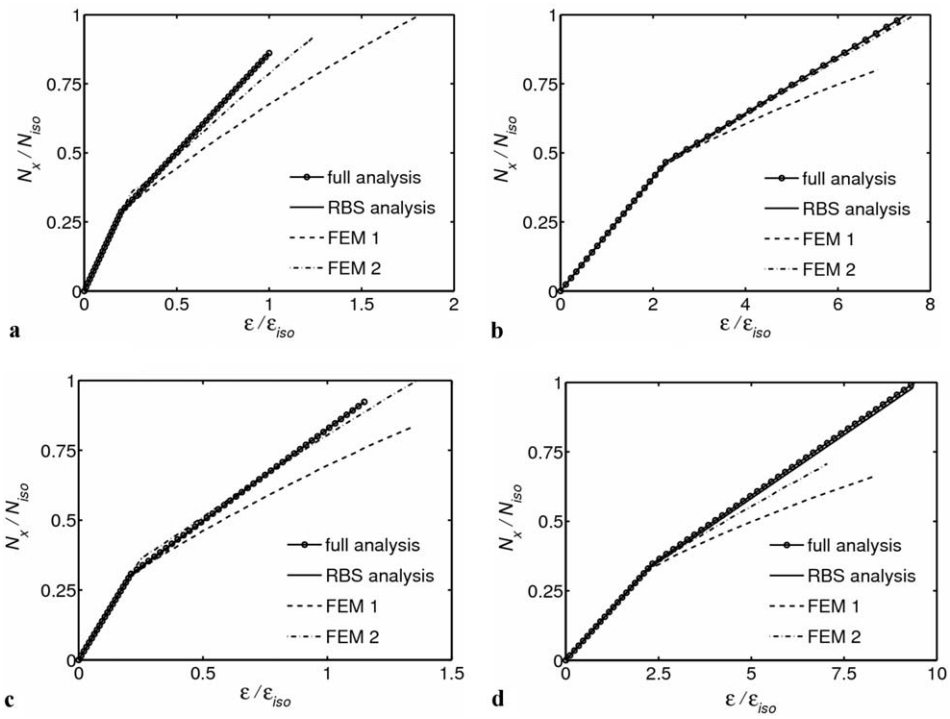

Fig. 7. Normalized strain $\varepsilon/\varepsilon_{\mathrm{iso}}$ function of the normalized axial loads N_x/N_{iso} for laminates made of two layers with 0, 90, 45 deg fiber angles: (a) [0/90], (b) [45/−45], (c) [0/45] and (d) [90/45].

Note that the nondimensional parameter η_B is associated with developing transverse curvature under axial load and may be thought of as an anisotropic Poisson's ratio. As such, plates with large values develop significant transverse curvature and at the point of buckling are no longer flat and may be better described as curved cylindrical panels. Thus, flat plate analysis is not necessarily the most appropriate modeling mechanism. Whether it is appropriate or not depends on the assumptions of classical plate theory, and, in particular, on the magnitude of transverse displacements, w. In this example, $w_{\max}/h \approx 0.37$, at the point of buckling, and as such, is small enough to be modeled as a flat plate. Regarding the approximate closed form solution, Fig. 6a and b shows identical results while Fig. 6c and d shows small differences between the full analysis and the RBS analysis. Moreover, note that in Fig. 6b for the angle-ply [45/−45] laminate configuration, for the postbuckling transverse displacement, an excellent match is found between the approximate solution and the FEM 2. This contradicts the results given by Ewing et al. (1988) regarding the RBS method and might be due to the fact that in Ewing et al. (1988) not all of the possible buckling modes were considered for the RBS method. Also, in Fig. 6a and c note the differences in the buckling loads between FEM 1 and FEM 2. In these figures, for the initial postbuckling response, the postbuckling transverse displacement given by the approximate solution lies between the results given by the two FEM analyses. Also, in Fig. 6d, for the [90/45] laminate configuration, the postbuckling transverse displacements given by the approximate solution are close to an averaged value of the results given by the two FEM analyses.

Fig. 7 shows the normalized strain $\varepsilon/\varepsilon_{\mathrm{iso}}$ as a function of the normalized axial loads N_x/N_{iso} for the same laminate configurations as in Fig. 6. Comparing the results given by the full analysis and the RBS analysis for the approximate solution, note, as in Fig. 6, identical results in Fig. 7a and b and small differences between them in Fig. 7c and d. Excellent agreement between the approximate solution analyses and the FEM analyses is observed for the prebuckling strain. Also, excellent agreement between the approximate solution analyses and the FEM 2 can be observed for the postbuckling strain in Fig. 7b for the angle-ply [45/−45] laminate configuration. In Fig. 7a and c, for [0/90] and [0/45] laminate configurations, respectively, the initial postbuckling strains given by the approximate solution lie between the results given by the two FEM analyses. Note

however that in Fig. 7d the initial postbuckling strains given by the approximate solution match FEM 2 only. Also, note the discrepancies for the postbuckling strain between the FEM 1 and FEM 2.

Fig. 8 shows the normalized maximum transverse displacement $w_{\max}/h$ as a function of the normalized axial loads N_x/N_{iso} for four laminates with two layers: [67.5/−67.5], [22.5/−22.5], [67.5/22.5] and [67.5/−22.5]. These layers are less used in practice but are nonetheless important for clarifying the validity of the approximate solution. For all the configurations, small differences exist between the results given by the full analysis and the RBS analysis for the approximate solution. In Fig. 8a and b, for the angle-ply laminate configurations [67.5/−67.5] and [22.5/−22.5], respectively, there is no prebuckling transverse displacement. Moreover, for the angle-ply laminate configurations, the approximate solution shows excellent agreement with FEM 2 for the postbuckling transverse displacement. Note in Fig. 8c, there is a large prebuckling transverse displacement for the [67.5/22.5] laminate configuration due to a large value of η_B, that is $|\eta_B| = 0.29$ for full analysis. Note that, at the point of buckling, the normalized maximum transverse displacement is $w_{\max}/h \approx 0.37$ and, as such, flat plate analysis is appropriate. Furthermore, for this laminate configuration, the postbuckling transverse displacements given by the approximate solution lie between the results given by FEM 1 and FEM 2. In Fig. 8d, for the [67.5/−22.5] laminate configuration, the prebuckling transverse displacement is very small. For this configuration, the approximate solution shows good agreements with FEM 2 but only for the initial path of the postbuckling transverse displacement. For higher axial compressive loads, the postbuckling transverse displacement given by FEM 2 is slightly larger than the transverse displacements given by the approximate solution.

Fig. 9 shows the normalized strain $\varepsilon/\varepsilon_{\text{iso}}$ as a function of the normalized axial loads N_x/N_{iso} for the same laminate configurations as in Fig. 8. As expected, excellent agreements between the approximate solution and the FEM analyses can be observed for the prebuckling strain. Also, for the initial path of the postbuckling strain, good agreements are found between the approximate solution and FEM 2, in Fig. 9c and d, for the [67.5/22.5] and [67.5/−22.5] laminate configurations, respectively. In these figures one can see very small differences between the full analysis and the RBS analysis for the approximate solution. On the contrary, in

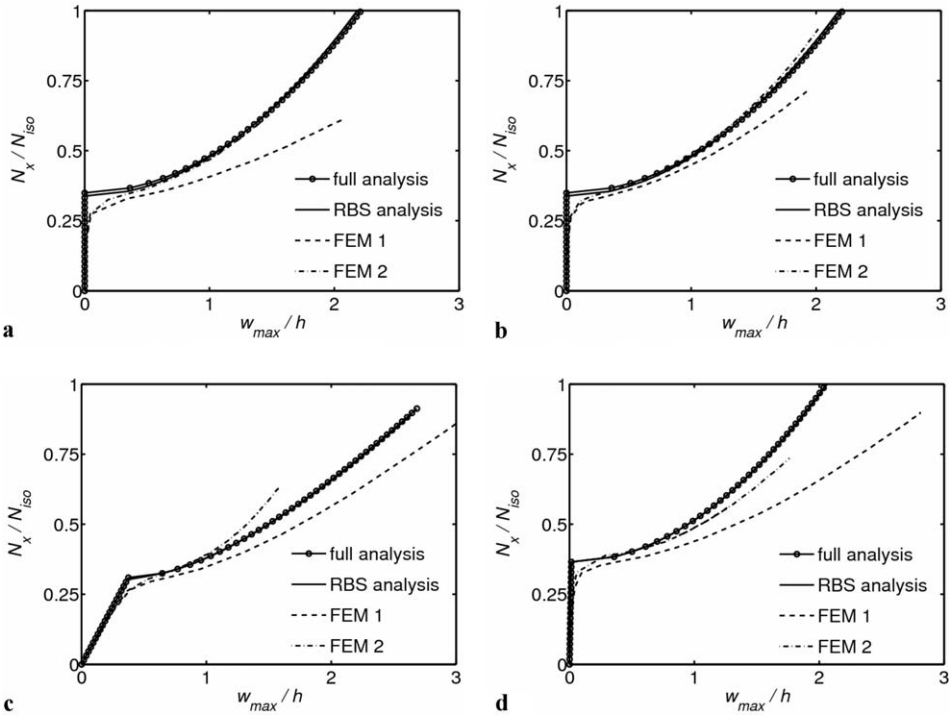

Fig. 8. Normalized maximum transverse displacement $w_{\max}/h$ function of the normalized axial loads N_x/N_{iso} for laminates made of two layers with 22.5 and 67.5 deg fiber angles: (a) [67.5/−67.5], (b) [22.5/−22.5], (c) [67.5/22.5] and (d) [67.5/−22.5].

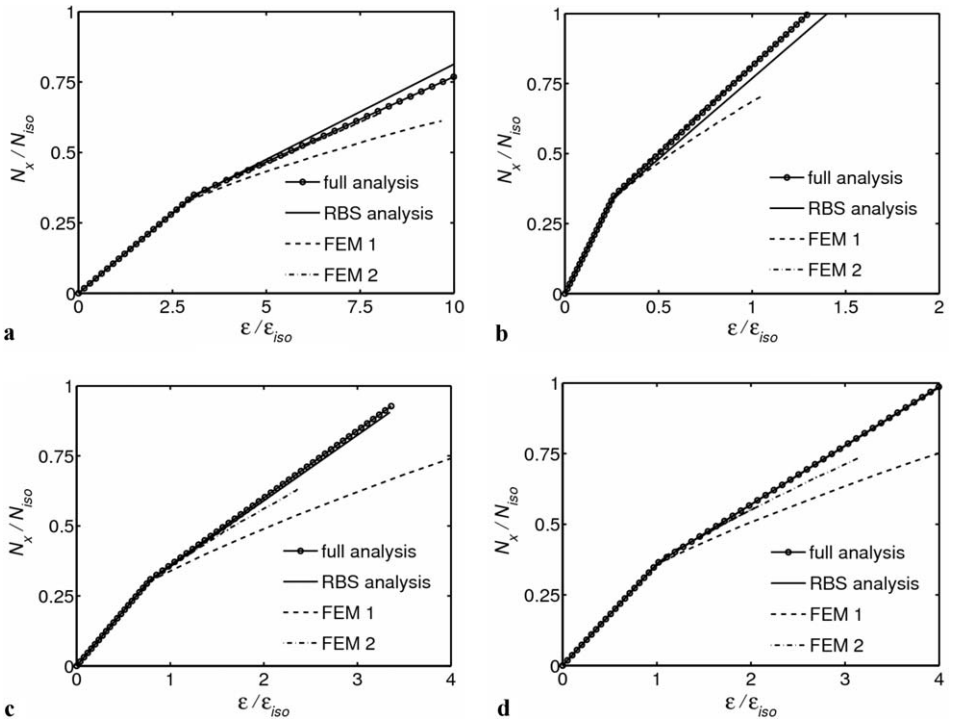

Fig. 9. Normalized strain $\varepsilon/\varepsilon_{iso}$ function of the normalized axial loads N_x/N_{iso} for laminates made of two layers with 22.5 and 67.5 deg fiber angles: (a) [67.5/−67.5], (b) [22.5/−22.5], (c) [67.5/22.5] and (d) [67.5/−22.5].

Fig. 9a and b, for the angle-ply configurations [67.5/−67.5] and [22.5/−22.5], respectively, the full analysis and the RBS analysis for the approximate solution show relatively large differences for the postbuckling strain due to different buckling wavelengths. However, the postbuckling strain given by the full analysis matches closely the postbuckling strain given by FEM 2. As in previous figures, the postbuckling strain given by FEM 1 is larger than the postbuckling strain given by FEM 2. Note in Fig. 9b that the postbuckling strain given by the RBS analysis for the approximate solution lies between the results given by FEM 1 and FEM 2.

Fig. 10 shows the normalized maximum transverse displacement w_{max}/h as a function of the normalized axial loads N_x/N_{iso} for eight laminates with four layers as combinations of 0, 90, 45 and −45 deg. To enforce a clear occurrence of buckling, a 2% imperfection was employed for FEM 2 in Fig. 10d for the [90/0/45/−45] laminate configuration. Except for the [45/90/−45/0] laminate configuration in Fig. 10h, for all the other configurations the prebuckling transverse displacement is large. Note in Fig. 10a, for the [0/0/45/−45] laminate configuration, in case of FEM 2 the plate buckles at a much larger axial load than in the case of the approximate solution or FEM 1. Also, the shape of the postbuckling transverse displacement given by FEM 2 suggests a different buckling mode than that assumed for the approximate solution. However, the results given by FEM 1 are much closer to the results given by the full analysis and by the RBS analysis for the approximate solution. Excellent agreement between the RBS analysis for the approximate solution and FEM 1 is observed for the postbuckling transverse displacement in Fig. 10b for the [90/90/45/−45] laminate configuration. Also, good agreement between the RBS analysis for the approximate solution and FEM 1 is observed for the postbuckling transverse displacement in Fig. 10d–g. In Fig. 10c, d and f, for the [0/90/45/−45], [90/0/45/−45] and [45/0/90/−45] laminate configurations, respectively, the RBS analysis shows postbuckling transverse displacements relatively larger than the full analysis for the approximate solution due to differences in the skew τ of the buckling pattern. For the other laminate configurations in Fig. 10, the differences between the postbuckling transverse displacements given by the RBS analysis and the postbuckling transverse displacements given by the full analysis are relatively small. One can see, in Fig. 10h, that for the [45/90/−45/0] laminate configuration, the full analysis for the approximate solution is in good agreement with FEM 2 but only for the initial

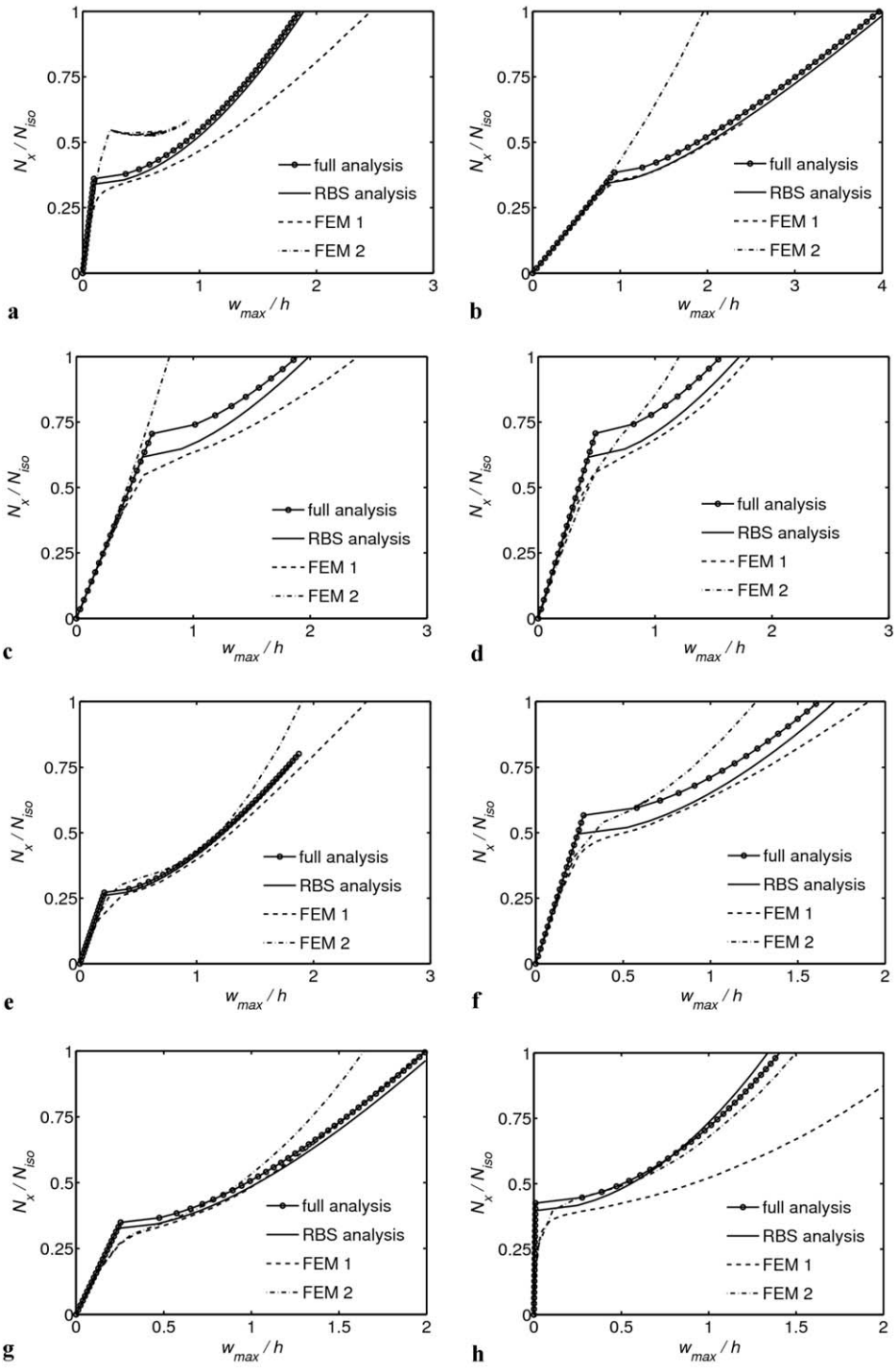

Fig. 10. Normalized maximum transverse displacement w_{max}/h function of the normalized axial loads N_x/N_{iso} for laminates made of four layers with 0, 90, 45 deg fiber angles: (a) [0/0/45/−45], (b) [90/90/45/−45], (c) [0/90/45/−45], (d) [90/0/45/−45], (e) [0/45/−45/90], (f) [45/0/90/−45], (g) [45/0/−45/90] and (h) [45/90/−45/0].

path of the postbuckling transverse displacement. Note that, in Fig. 10b and c, for [90/90/45/−45] and [0/90/45/−45] laminate configurations, plates do not buckle for the FEM 2 analysis. For these configurations, the

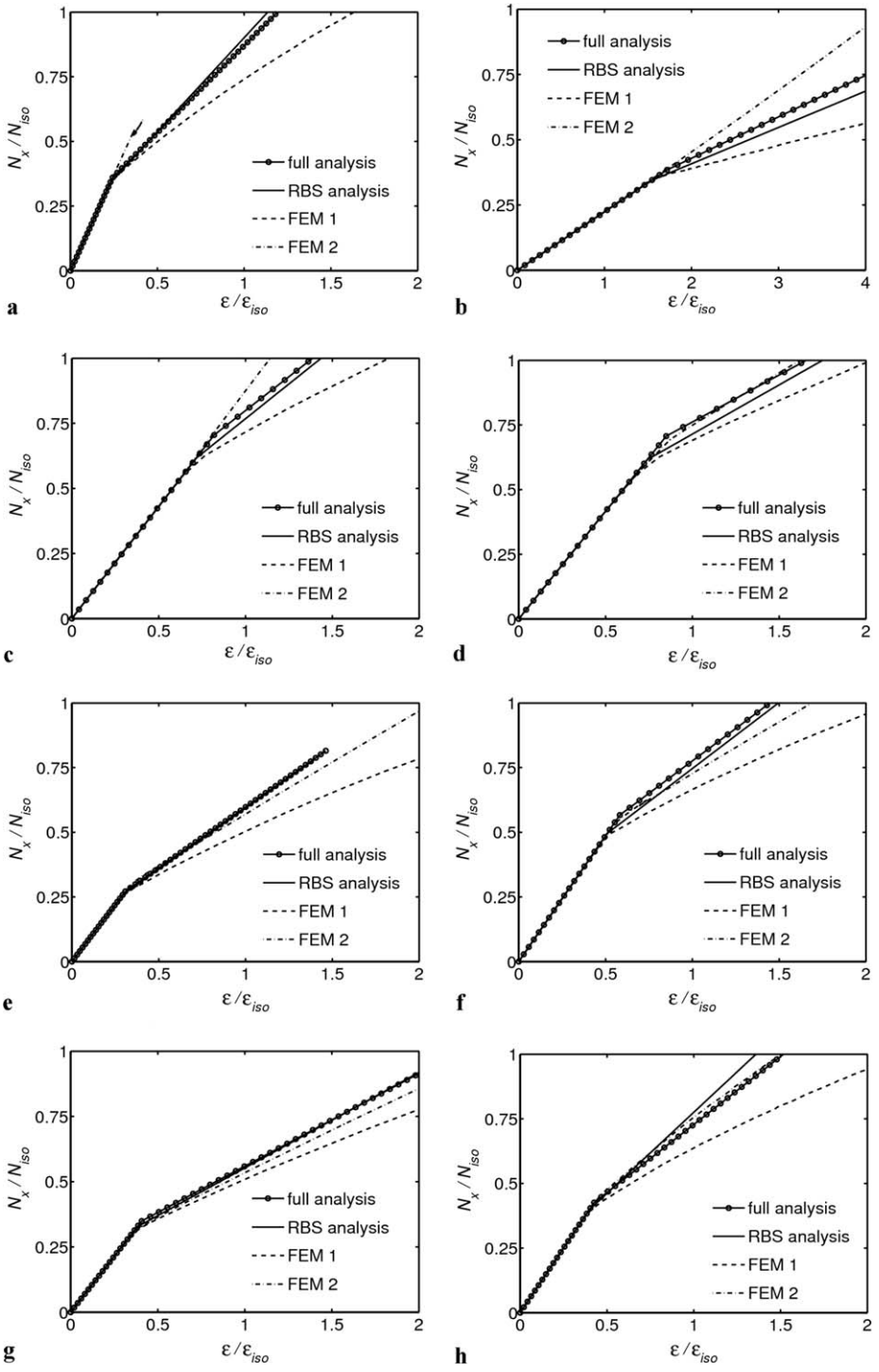

Fig. 11. Normalized strain $\varepsilon/\varepsilon_{\text{iso}}$ function of the normalized axial loads N_x/N_{iso} for laminates made of four layers with 0, 90, 45 deg fiber angles: (a) [0/0/45/−45], (b) [90/90/45/−45], (c) [0/90/45/−45], (d) [90/0/45/−45], (e) [0/45/−45/90], (f) [45/0/90/−45], (g) [45/0/−45/90] and (h) [45/90/−45/0].

nondimensional coupling parameter η_B takes very large values, for full analysis these values are $|\eta_B| = 1.15$ and $|\eta_B| = 0.47$, respectively. Also, the normalized maximum transverse displacements are $w_{\max}/h \approx 0.84$

and $w_{max}/h \approx 0.56$, respectively, at the point of buckling in the RBS analysis. These plates have developed significant transverse curvature and, in the case of straight longitudinal edges (i.e. FEM 2), have developed periodic transverse direct stresses that appear to delay the onset of buckling.

Fig. 11 shows the normalized strain $\varepsilon/\varepsilon_{iso}$ as a function of the normalized axial loads N_x/N_{iso} for the same laminate configurations as in Fig. 10. In Fig. 11, the discrepancies between the postbuckling strain given by the full analysis and the RBS analysis for the approximate solution are due to different buckling wavelengths. In Fig. 11a–c, the postbuckling strains given by the full analysis and the RBS analysis lie between the results given by FEM 1 and FEM 2 analyses. In Fig. 11d, for the [90/0/45/−45] laminate configuration, only the postbuckling strain given by the RBS analysis lies between the results given by FEM 1 and FEM 2 analyses. The postbuckling strain given by the full analysis matches the postbuckling strain given by FEM 2. In Fig. 11e–h, the initial path of the postbuckling strains given by the RBS analysis for the approximate solution lie near the results given by FEM 2 and do not match the results given by FEM 1. In Fig. 11f, for the [45/0/90/−45] laminate configuration, the full analysis gives the smallest postbuckling strain in comparison with RBS analysis, FEM 1 and FEM 2. In Fig. 11h, for the [45/90/−45/0] laminate configuration, the full analysis gives postbuckling strain larger than RBS analysis and FEM 2. Note in Fig. 11b and c that the laminate fails to buckle with FEM 2 analysis. Also, note in Fig. 11a for the [0/0/45/−45] laminate configuration, the very short path for the postbuckling strain given by FEM 2. For this laminate configuration, due to the convergence criteria required in the FEM postbuckling analysis, the FEM 2 analysis could not be pursued beyond the maximum load shown in Fig. 11a (or indeed Fig. 10a).

5. Conclusions

Nondimensional parameters were used to express in a very simple and clear formulation the approximate solution for the postbuckling of infinitely long unsymmetrically laminated composite plates. One can understand and identify the importance of each of the nondimensional parameters for the postbuckling problem. For unsymmetric laminate configurations an important coupling nondimensional parameter to be taken into consideration is η_B. Laminated plates with increasingly larger values of η_B increasingly behave as curved cylindrical panels, and as a result, may have larger buckling loads depending on the nature of boundary conditions on the longitudinal edges. For the postbuckling problem, the RBS method can be adopted in order to reduce the complexity of the solution.

In order to study and validate the approximate solution for postbuckling problem, the results obtained by the approximate solution for infinitely long plates are compared with the results obtained by FEM for finite length rectangular plates of representative unsymmetric laminate configurations. The influence of the boundary conditions on postbuckling response is also studied. For the FEM analysis, two different simply supported boundary conditions on the long edges of the plate are considered. The first FEM analysis is carried out for plates with the simply supported lateral edges without any straightness constraint imposed on them while the second FEM analysis is carried out for plates with the simply supported lateral edges forced to remain straight. These two sets of boundary conditions give different results for the buckling and postbuckling finite element analyses.

The approximate solution using the full analysis also the RBS analysis, gives good results for unsymmetrically laminated angle-ply plates subjected to axial compression. These results are in excellent agreements with the results given by the FEM analysis for plates with the simply supported lateral edges forced to remain straight. For other laminate configurations, in most cases the two FEM analyses overestimate and, respectively, underestimate the results given by the approximate closed form solution, depending on the type of simply supported boundary condition considered. Also, in many cases, the analysis employing RBS method simplifications is very near or more conservative than the analysis taking into consideration all the coupling terms. Thus, the approximate solution appears useful for initial design purposes as an averaged quantity between the two FEM analyses.

References

Ashton, J.E., 1969. Approximate solutions for unsymmetrical laminated plates. Journal of Composite Materials, 189.
Chandra, R., 1988. Postbuckling analysis of cross-ply laminated plates. AIAA Journal 13, 1388–1399.

Chia, C.Y., Prabhakara, M.K., 1974. Postbuckling behaviour of unsymmetrically layered anisotropic rectangular plates. Journal of Applied Mechanics 41 (3), 155–162.

Diaconu, C.G., Weaver, P.M., 2005. Approximate solution and optimum design for postbuckling of axially compressed laminated composite plates. AIAA Journal 43 (4), 906–914.

Ewing, M.S., Hinger, R.J., Leissa, A.W., 1988. On the validity of the reduced bending stiffness method for laminated composite plate analysis. Composite Structures 9, 301–317.

Harris, G.Z., 1975. The buckling of and postbuckling behavior of composite plates under biaxial loading. International Journal of Mechanical Sciences 17, 187–202.

Kromm, A., Marguerre, K., 1937. Behaviour of a plate strip under shear and compressive stresses beyond the buckling limit. Technical Memorandums NACA, no. 870.

Lagace, P.A., Jensen, D.W., Finch, D.C., 1986. Buckling of unsymmetric composite laminates. Composite Structures 5, 101–123.

Pope, G.G., 1968. On the bifurcational buckling of elastic beams, plates and shallow shells. Aeronautical Quarterly 19, 20–30.

Prabhakara, M.K., 1976. Post-buckling behaviour of simply-supported cross-ply rectangular plates. Aeronautical Quarterly 27, 309–316.

Qatu, M.S., Leissa, A.W., 1993. Buckling or transverse deflections of unsymmetrically laminated plates subjected to in-plane loads. AIAA Journal 31 (1), 189–194.

Stein, M., 1983. Postbuckling of orthotropic composite plates loaded in compression. AIAA Journal 21 (12), 1729–1735.

Timoshenko, S., 1913. Sur la Stabilite des Systemes Elastiques. Annales des Ponts et Chaussees, 9th Series, vol. 17(V) (September–October), pp. 372–412.

Turvey, G.J., Wittrick, W.H., 1973. The large deflection and post-buckling behaviour of some laminated plates. Aeronautical Quarterly 24, 77–86.

Weaver, P.M., 2004. On optimization of long anisotropic flat plates subject to shear buckling loads. In: 45th AIAA/ASME/ASCE/AHS/ACS Structures, Structural Dynamics & Materials Conference, 19–22 April, Palm Springs, CA.

Weaver, P.M., 2006. Approximate closed-form solution for buckling of compression loaded laminated rectangular plate with flexural/twist anisotropy. Proceedings of the Royal Society A 462 (2065), 59–73.

Zhang, Y., 1982. Buckling and Postbuckling Behaviour of Generally Layered Composite Panels. Ph.D. Dissertation, Department of Aeronautics, Imperial College, London.